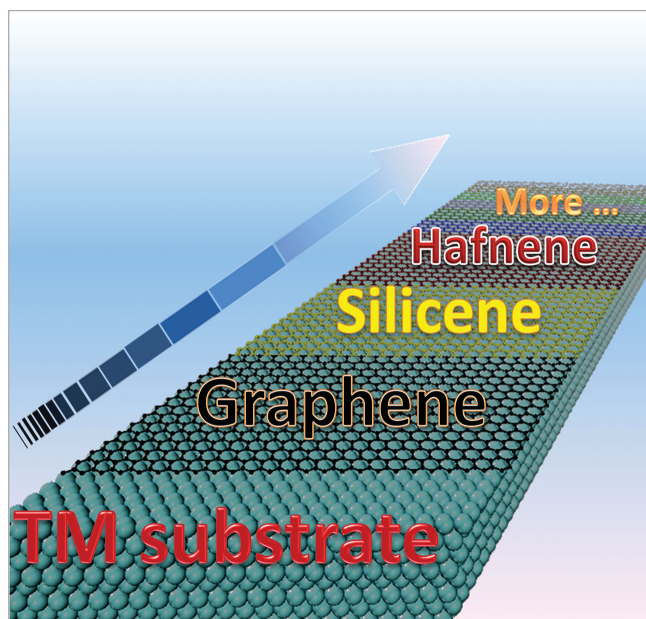# Construction of 2D Atomic Crystals on Transition Metal Surfaces: Graphene, Silicene, and Hafnene

Yi Pan, Lizhi Zhang, Li Huang, Linfei Li, Lei Meng, Min Gao, Qing Huan, Xiao Lin, Yeliang Wang, Shixuan Du,* Hans-Joachim Freund, and Hong-Jun Gao*

From the Contents

The synthesis and structures of graphene on Ru(0001) and Pt(111), silicene on Ag(111) and Ir(111) and the honeycomb hafnium lattice on Ir(111) are reviewed. Epitaxy on a transition metal (TM) substrate is a promising method to produce a variety of two dimensional (2D) atomic crystals which potentially can be used in next generation electronic devices. This method is particularly valuable in the case of producing 2D materials that do not exist in 3D forms, for instance, silicene. Based on the intensive investigations of epitaxial graphene on TM in recent years, it is known that the quality of graphene is affected by many factors, including the interaction between the 2D material overlayer and the substrate, the lattice mismatch, the nucleation density at the early stage of growth. It is found that these factors also apply to many other epitaxial 2D crystals on TM. The knowledge from the reviewed systems will shine light on the design and synthesis of new 2D crystals with novel properties.

1. Introduction

Two dimensional atomic crystals have crystalline and macroscopic scales in two dimensions but only one or a few atomic layers in the third dimension. They are usually (but not necessarily) obtained by exfoliating their parent crystals, which have weak interaction between the neighboring layers, *i.e.*, the van der Waals solids.[1–3] Due to their unique structures, the 2D atomic crystals typically have special physical properties or chemical reactivities.[4,5] In addition, these properties can sometimes be precisely regulated or even tailored by modifying the structures or chemical compositions.[6] Therefore, these materials exhibit very promising potential applications, for instance, in the next generation electronic devices and the nanoscale chemical sensors.[7–9]

The research on the 2D atomic crystals has been increasing extremely fast since the debut of graphene in 2004.[2,10] Up to now, dozens of 2D atomic crystals have been successfully synthsized. Most of them can be classified into three categories according to their chemical compositions.[11–13] The first category is the graphene family, including graphene, silicene, h-BN, BCN and chemically modified graphene, which all have honeycomb structures.[14,15] These materials, especially graphene, have been intensively studied in both fundamental and applied aspects. Many synthesis methods have been developed, some of which can almost fulfill the requirements of industry.[16–18] And, lots of model devices based on these materials have been fabricated.[8,19]

The second category is the 2D dichalcogenide family, including transition metal disulfides, ditellurides and diselenides.[20–22] Although some of them, for example, MoS_2, have been well studied, most of them have just begun to get attention.[21–23]

The third category includes some TM oxides and hydroxides that are stable in the single- or few-layered 2D form.[1,12,13] These materials are not as stable as the ones from the other two categories in ambient conditions; therefore the synthesis is more difficult. Owing to the contributions of electrons in *d* and *f* orbitals, these materials are believed to have some interesting physical properties that need to be further investigated.[12] Apart from the three categories, there are some new types of 2D crystals. For example, the recently reported epitaxial 2D honeycomb lattice of hafnium synthesized on Ir(111), does not belong to any of the three categories.[24] There are still many new 2D atomic crystals to be explored.

Since most of the 2D crystals have a 3D counterpart, i.e., parent materials, they usually can be prepared by exfoliation from their parent materials. The original exfoliation method invented by Geim's group relies on mechanical force to peel off the layers.[1] This method is very effective for many graphene family materials, but not very efficient. Many new exfoliation methods which are more suitable for mass production have been developed later.[15,21,22,25,26] The most widely used ones are the chemical exfoliation methods, in which the weak van de Waals bonds between the layers of the parent materials are opened by intercalating small molecules in gas phase or ions in solutions into the space between the layers. While large amount of graphene family materials and metal disulfides can be produced by exfoliation,[17,21,26] 2D crystals can also be directly synthesized from precursors.[12,18,27,28] The main direct chemical synthetic strategy is connecting the building blocks by self-assembly, oriented attachment or template directed attachment, which have been widly used for synthesizing many TM chalcogenides and oxides.[12]

Another important direct synthetic strategy is epitaxial growth of 2D crystal on the surface of a well-chosen substrate by chemical vapor deposition (CVD) or physical vapor deposition (PVD).[29–35] Epitaxial growth on a TM substrate is an effective way to synthesize a variety of two dimensional atomic crystals of the graphene family. It has some unique advantages over the methods that rely on the corresponding 3D crystals as parent material. Due to the advantages of clean synthesis environments and the high quality of the products, the CVD and PVD methods are especially suitable for producing a 2D material that can be transferred to silicon wafers and used in electronic devices.[17,34,36,37] The epitaxy method is particularly valuable in the case of producing 2D materials that do not exist in 3D form, like the silicene. Interestingly, although each individual 2D crystal has its own unique properties, the various epitaxial 2D crystals are similar in many aspects, implying the knowledge from the intensively studied systems can be used to guide the synthesis of new materials.

In this review, we focus on the synthesis of 2D atomic crystals on TM substrates by means of epitaxial growth in the ultra high vacuum (UHV) environment. The main investigation method referenced in this paper is scanning tunneling microscopy (STM).[38] In the first section, the factors that govern the quality of epitaxial graphene on TM surfaces are discussed, followed by a case study of graphene on Ru(0001) and Pt(111). In the second section, taking the Ir(111) and Ag(111) substrates as examples, the silicene-TM system is discussed . In the last section, the application of this method to the new hafnium 2D crystals is discussed.

Dr. Y. Pan, Dr. L. Z. Zhang, Dr. L. Huang, L. F. Li,
Dr. L. Meng, Dr. M. Gao, Dr. Q. Huan,
Prof. Y. L. Wang, Prof. S. X. Du,
Prof. H.-J. Gao
Institute of Physics & University of
Chinese Academy of Sciences
Chinese Academy of Sciences
Beijing 100190, China
E-mail: sxdu@iphy.ac.cn; hjgao@iphy.ac.cn

Dr. Y. Pan, Prof. H.-J. Freund
Fritz-Haber-Institut der Max-Planck-Gesellschaft
Faradayweg 4–6
D-14195, Berlin, Germany

Dr. L. Huang
Institute of Chemistry
Chinese Academy of Sciences
Beijing 100190, China

Dr. X. Lin
University of Chinese Academy of Sciences & Institute of Physics
Chinese Academy of Sciences
Beijing 100190, China

2. Epitaxial Graphene on TM Surfaces

Graphene was found to be formed on TM single crystal surfaces as early as in the 1960s.[39] For a couple of decades, such carbon deposits were mainly viewed as annoying contaminants that had to be removed from the TM surfaces. Since the rise of graphene in the new century, many scientists realized the significance of this material and revisited the graphene-TM systems. Up to the writing of this paper, more than a dozen different TM surfaces have been used as substrates to grow epitaxial graphene.[27,29,32,36,40–44] In particular, it was found that even some polycrystalline TM films are good enough for the synthesis of large scale graphene flakes of pretty high quality by means of CVD, which could dramatically reduce the cost of graphene production.[34,35,45] The as prepared epitaxial graphene can be decoupled from the substrate by etching the substrate or intercalating foreign atoms into the graphene-TM interface.[35,46,47] In addition, thanks to the high quality of epitaxial graphene and the significant improvement of the techniques for transferring epitaxial graphene from TM surfaces to any substrate surface, this method is considered to be one of the most promising methods for the future industrial production of graphene.[17,34,35,37]

In this section we first review the factors that influence graphene quality, then discuss the details of graphene grown on two typical TM substrates, Ru(0001) and Pt(111), which have strong and weak interaction with graphene, respectively.

2.1. The Factors That Influence Graphene Quality

Although graphene can be synthesized on many TMs, the quality and properties of graphene on different TM substrates varies due to many factors.

The most important factor that influences the quality of graphene on a TM substrate is the interaction between the graphene and the TM. If the interaction is strong, graphene islands that form at the initial stage of growth all have the same orientation, and thus they can connect to each other seamlessly during growth and form a single 2D crystal with very low density of defects. However, the electronic structure of the graphene will be affected by its interaction with the TM substrate. In contrast, if the interaction is weak, the islands formed at the initial stage have different orientations, so the final graphene film has numerous small rotational domains and high density of defects at the domain boundaries. But the inherent physical properties of the graphene might be largely preserved in this case.

Another important factor is the lattice mismatch between graphene and a TM substrate. If the lattice mismatch is large, the graphene film is usually corrugated due to the inhomogenous interaction of the carbon atoms with the substrate.[48] The leval of corrugation depends on the strength of the interaction. As shown in the STM images in **Figure 1**(a)-(e), the corrugation of graphene on these substrates increases in such an order: graphite < Pt(111) < Ir(111) < Rh(111) < Ru(0001).[41–43,47,49,50] It has been proved by X-ray photoelectron spectroscopy (XPS) that the interaction of these substrates with graphene increases in the same order.[48] In

Yi Pan received his Ph.D. in physics from the Institute of Physics, Chinese Academy of Sciences in 2011. He subsequently held postdoctoral positions in the Fritz Haber Institute and the Paul Drude Institute for Solid State Electronics, in Germany. His research interests focus on the structure and physical properties of low-dimensional nano-materials.

Shixuan Du studied at Peking University (B.S.), and received her Ph.D. in physical chemistry from Beijing Normal University in 2002. After that, she joined the Nanoscale Physics and Devices Laboratory of the Institute of Physics, Chinese Academy of Sciences. She became a Professor of the Institute of Physics in 2009. Her research interests focus on the DFT calculations for the structural, physical and dynamic properties of molecules on metal surfaces.

Hong-Jun Gao received his Ph.D. in physics from Peking University in 1994. After that, he joined the Nanoscale Physics and Devices Laboratory of the Institute of Physics, Chinese Academy of Sciences. He became a Professor of the Institute of Physics in 1995. Now, he is an Academician of the Chinese Academy of Sciences and an Academician of the Developing-Country Academy of Sciences. His research interest is on the construction and physical property of low-dimensional nanostructures, and scanning tunneling microscopy/spectroscopy .

addition, the C 1s peak of graphene splits in the case of a strong interaction (Figure 1 (f)), indicating the chemical environment of some carbon atoms in the graphene is changed due to the strong interaction. Therefore, the good electronic properties are affected as well. On the other hand, a smaller lattice mismatch gives rise to flatter graphene film, for example, graphene on Ni(111).[51]

The quality of epitaxial graphene on TM surfaces is also influenced by some kinetic factors during the growth process.[33,52] Take the nucleation rate as an example, dense nucleation results in a graphene sample with small domains and a high density of defects, while sparse nucleation dramatically improves the quality of graphene by enlarging the domain size.[43] The nucleation rate is normally controlled by changing the precursor partial pressure. The surface impurities of the substrate can also play an important role, for instance, the surface oxygen on copper substrate.[70]
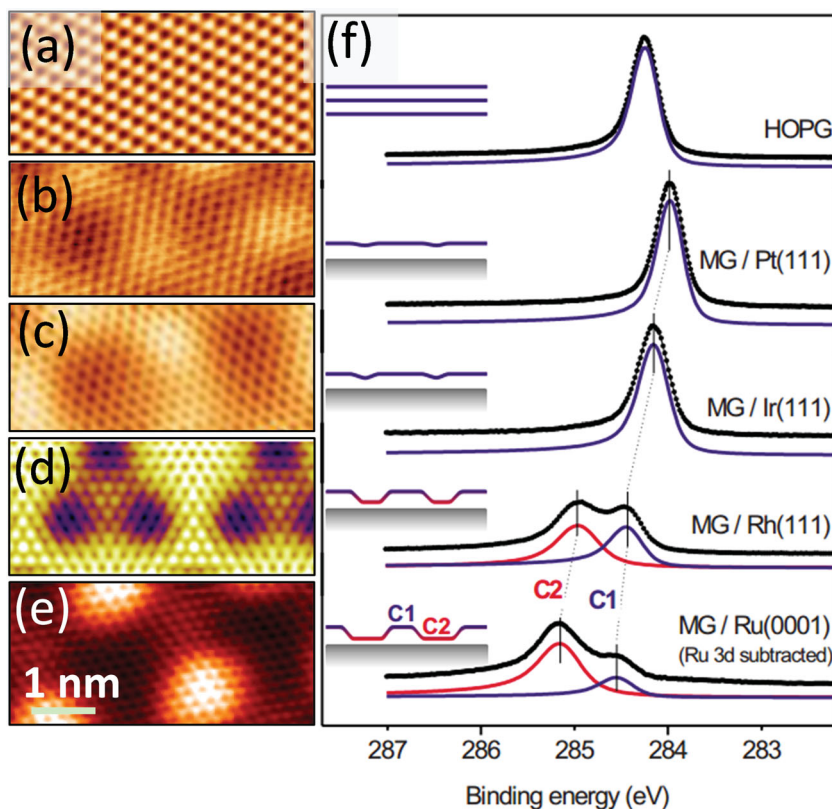
Figure 1. STM images and photoelectron spectra of graphene on different substrates. STM images of (a) graphite and (b)-(e) graphene on Pt(111),[43] (Copyright 2011, American Institute of Physics) Ir(111),[47] (Copyright 2012, American Institute of Physics) Rh(111)[42] (Copyright 2012, American Institute of Physics) and Ru(0001).[41] (Copyright 2009, Wiley-VCH) The STM images are of the same scale. (f) C 1s photoelectron spectra taken in normal emission graphite and graphene on the TM surfaces.[48] (Copyright 2008, American Physics Society) All panels reproduced with permission.

In addition, the three most common carbon sources for graphene grown on TM, internal carbon contained in the TM substrate, external carbon from a hydrocarbon precursor, and a pure carbon source in an evaporator, would result in graphene films of different thicknesses. The graphene prepared by hydrocarbon decomposition is normally with a single layer. This is because the decomposition reaction occurs only on a bare TM surface, and consequently the growth is a self-terminating process that stops when the TM surface is fully covered by a single layer of graphene.[53] On the other hand, if the graphene is prepared from the other two carbon sources, the vetical growth would not stop until the supply of surface carbon is terminated, consequently the multilayer graphene can be formed.[52]

2.2. Single Crystalline Graphene on Ru(0001)

The graphene shown in **Figure 2** is synthesized by annealing a ruthenium single crystal substrate containing small amount of carbon (approximately 15 ppm).[41] Graphene grows on Ru(0001) surface when carbon is segregated from the bulk of the substrate by annealing. The annealing process is as follows: slowly ramping the temperature of the ruthenium substrate to 1000 K; maintaining such temperature for 20 min; slowly cooling to room temperature. The carbon segregation is confirmed by comparing the carbon signal on the Auger electron spectroscopy (AES) and XPS spectra before and after annealing. The AES and XPS also indicate that no other new elements appear on the substrate surface after annealing.

The low energy electron diffraction (LEED) pattern of bare and graphene covered Ru(0001) are shown in Figure 2(a) and (b), respectively. Compared with the simple hexagonal pattern of bare Ru(0001), the graphene overlayer shows more diffraction spots at the same electron beam energy, indicating a superstructure on the surface, i.e., the moiré pattern on an incommensurate superstructure. Since the spots in the graphene LEED pattern have the same orientation as the ones of the Ru(0001) substrate, the moiré pattern is solely from the lattice mismatch, hereby about 10%. The typical LEED pattern in Figure 2(b) does not change with the measuring place on the sample, implying that the highly crystalline 2D lattice is very homogenous. The most important infomation from the LEED pattern is that there is only one preferred orientation of epitaxial graphene on Ru(0001), which enables the formation of a macroscopic single crystalline graphene.

The atomic level structure of graphene on Ru(0001) was studied with STM. Figure 2(c) is an overview STM image showing that terraces on the sample are clean and smooth. But the zoomed-in STM image of the terrace, Figure 2(d), reveals that the surface has periodical protrusions, forming a hexagonal array. This structure is the moiré pattern which is already revealed by the LEED pattern in Figure 2(b). The moiré pattern on all the terraces is oriented in the same direction. The average distance between the neighboring moiré spots is 3 nm, which is about 12 times the lattice constant of graphene and 11 times that of Ru(0001).

The atomic structure of the graphene is shown in the high resolution image in Figure 2(e). The rhombus encloses a unit cell of the moiré pattern. Within each unit cell, the superlattice consists of three structural regions: the hill region (marked by the green circle in Figure 2(e)) is bowed up into a ridge, the valley region (marked by the yellow dashed triangle) is bowed down into a valley, and the intermediate region (marked by the blue dotted triangle) is of medium height. A corresponding ball model of a unit cell is shown in Figure 2(f), which clearly indicates the different sites where the carbon atoms sit. In the valley region, all the carbon atoms sit right on top of Ru atoms, implying that the smaller graphene-Ru distance is caused by the relatively larger interaction between carbon and ruthenium in this region. But in
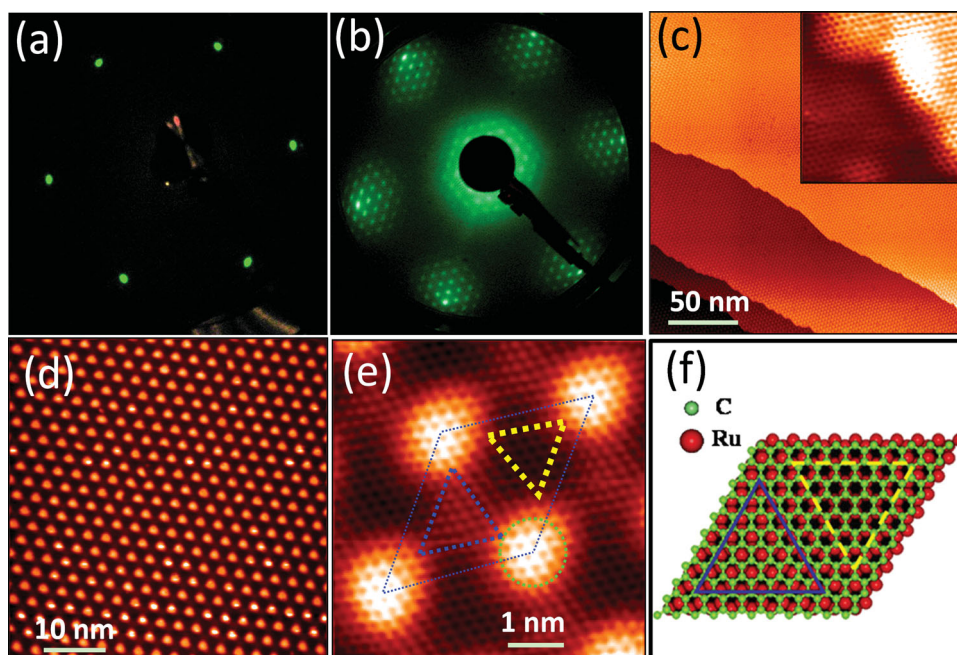
Figure 2. Graphene on Ru(0001). (a) LEED pattern of clean Ru(0001) and (b) graphene on Ru(0001), the electron beam energy is 60 eV. (c–e) STM images of graphene on Ru(0001). The inset in (c) shows graphene at a step edge of the substrate. The rhombus in (e) indicates a unit cell of the moiré pattern, in which the three different regions are marked by the circle and triangles. (f) Atomic model of graphene on Ru(0001) in a unit cell. Tunneling parameters: (c) $V_{bias} = 1.2$ V, $I = 0.17$ nA; (d) $V_{bias} = -1.2$ V, $I = 0.35$ nA; and (e) $V_{bias} = -0.46$ V, $I = 0.27$ nA. Reproduced with permission.[41] (Copyright 2009, Wiley-VCH).

the hill region, all the carbon atoms sit on the hollow site of the substrate, implying a larger graphene-Ru distance caused by a relatively smaller C-Ru interaction. This hypothesis has been confirmed by DFT calculations.[54] In addition, interaction variation in such a moiré unit cell is further confirmed in other situations by site specific adsorption of metal clusters and molecules in a unit cell of such surfaces.[55]

Another important finding is that the graphene lattice is continuous over substrate steps with no interruption of its structure. The small image inserted in Figure 2(c) is an STM image taken at a step-edge area, showing that the graphene overlayer remains perfectly crystalline over the Ru step without bond-breaking or defects. These results indicate that high quality 2D graphene crystals with larger size can be synthesized even if the substrate terraces are narrow. Similarly, high quality epitaxial graphene has been successfully synthesized even on polycrystalline copper substrates.[36]

2.3. Multi-Domain Graphene on Pt(111)

Epitaxial graphene on Pt(111), shown in **Figure 3**, has been synthesized by decomposition of ethylene at an elevated temperature.[43] The samples are prepared by exposing clean Pt(111) surface to high purity ethylene while the Pt substrate is heated to 1073 K.[43] The partial pressure of ethylene is 5×10^{-7} mbar and the exposure lasts 100 s.

As shown in the LEED pattern in Figure 3(a), the diffraction pattern of graphene is composed of sharp arcs, indicating that the graphene has a unique periodicity but many

preferred orientations. This means the 2D crystal of graphene is polycrystalline with many rotational domains.

The morphology of the polycrystalline graphene on Pt(111) was studied with STM. The overview STM image in Figure 3(a) shows that the roughness of the surface is due to a high density of defects (short lines, protrusions and holes). The close-up images in Figure 3(b) reveal that these defects are mainly located at the domain boundaries, indicated by the dashed lines. Within the domains, the surface is smoother and shows typical hexagonal moiré patterns.

The orientation and periodicity of the moiré pattern varies with the rotation angle of the graphene in each domain. Based on the moiré pattern's orientation with respect to the graphene lattice's orientation, six typical moiré superstructures are found. In Figure 3(c) upper panels the lattice vectors of moiré superstructures are parallel to the lattice vector of graphene, as in the 2×2, 3×3, and 4×4 domains shown. The corrugation of these domains is within 0.03 nm, indicating the graphene film is very flat without much distortion in the vertical direction. The lower panels of Figure 3(c) show three rotational domains in which the lattice vectors of the moiré superstructures are not aligned with the graphene lattice vector. The corrugation of these domains is 0.05–0.08 nm. Nevertheless, these corrugations are much smaller than those of graphene on Ru(111).

Compared with graphene on Ru(0001), the density of defects is very high even inside the domains. The domain size varies from a few to tens of nanometers. The domain size can be bigger if the nucleation density is reduced at an early stage of graphene growth. Indeed, an average domain size
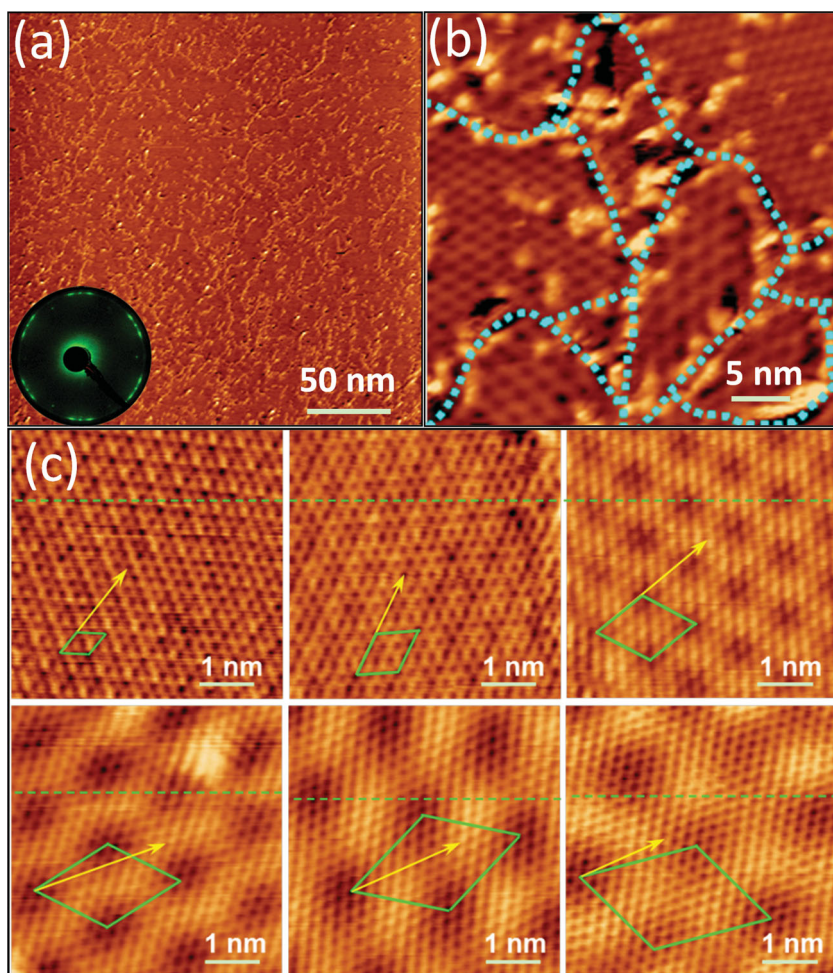
Figure 3. STM images of graphene on Pt(111) with (a) large area, (b) different domains and (c) typical rotational domains: upper row: 2 × 2, 3 × 3, and 4 × 4; lower row: ($\sqrt{37} \times \sqrt{37}$) R21°, ($\sqrt{61} \times \sqrt{61}$) R26°, and ($\sqrt{67} \times \sqrt{67}$) R12°. The inset in (a) shows the LEED pattern. The dashed lines in (b) indicate the domain boundaries. The [$2\bar{1}\bar{1}0$] direction of graphene lattices is indicated by the yellow arrows and moiré unit cells are in green rhombuses. Reproduced with permission.[43] (Copyright 2011, American Institute of Physics).

of about one hundred nanometers has been observed in epitaxial graphene grown with sparse nucleation.[43] However, the polycrystallinity is unavoidable for epitaxial graphene on Pt(111).[43,50]

The dramatic difference between graphene-Ru(0001) and graphene-Pt(111) systems is mainly attributed to the interaction between the graphene and the substrate. In addition, the nucleation density also plays a role. For mass production of high quality large scale graphene by means of TM surface epitaxial methods, all the important factors discussed in section 2.1 need to be considered.

3. Epitaxial Silicene on TM Surfaces

Silicene is a 2D atomic crystal which has a honeycomb structure similar to that of graphene, but made up of silicon atoms rather than carbon atoms. It has attracted much interest of scientists because it is expected to have many useful physical properties, for instance the quantum spin Hall effect.[56] The

concept of silicene originated with theoreticians when they constructed a model of free-standing single-layer.[57] Because of the large Si-Si bond length and the partial sp^3 hybridization, free-standing silicene is always nonplanar, in a so-called low-buckled geometry. The silicene sample cannot be prepared through the exfoliation method because no parent material exists for silicene. Therefore the primary method to synthesize silicene sheets is epitaxial growth of silicon on solid surfaces. Recently, the silicene strips and films have been successfully synthesized on TM substrates, for example, Ag(110), Ag (111), Ir(111) and zirconium diboride (ZrB$_2$) thin films supported on Si wafers.[30,58–74] The silicene on Ir(111) has only one phase with large rotation domains.[60,61] But the silicene on Ag(111) has much more complicated phases and domains.[31,62–65,72] Similar to the graphene-TM systems, the exceptional behavior of silicene is mainly attributed to the interaction with the substrate. In this section, we review the epitaxial silicene on Ir(111) and Ag(111) surfaces.

3.1. Silicene on Ir(111)

The epitaxial silicene on Ir(111) surface shown in **Figure 4** is synthesized by depositing silicon on the Ir(111) surface and post annealing at 400 °C for 30 min.[61] The LEED pattern of the sample is shown in Figure 4(a). The spots highlighted by the yellow dashed circles are assigned to the Ir(111) substrate. The silicene diffraction spots can be separated into two identical patterns with different orientations, as shown in the sketch map in Figure 4(b), in which the spots are in two colors for the two domains. Each domain can be identified as a ($\sqrt{7} \times \sqrt{7}$) superstructure with respect to the Ir(111) substrate. The corresponding angles between Ir[$1\bar{1}0$] and the high symmetry direction of ($\sqrt{7} \times \sqrt{7}$) of the two silicene domains are 40.9° and 19.1°, respectively.

The STM images in Figures 4(c) and (d) show two silicene rotational domains that are obtained at different locations on the same sample. The angles between the orientations of the two domains and the Ir[$1\bar{1}0$] direction are 40.9° and 19.1°, respectively. This is consistent with the two equivalent domains detected in ($\sqrt{7} \times \sqrt{7}$) LEED patterns in Figure 4(a). The overview image in Figure 4(c) shows a long-range ordered hexagonal lattice of protrusions. Figure 4(e) shows the line profile along the black line in Figure 4(d). The periodicity of the bright protrusions in the STM image is about 0.72 nm, which is $\sqrt{7}$ times the Ir(111) lattice constant (0.271 nm). The height of the protrusions in the silicene
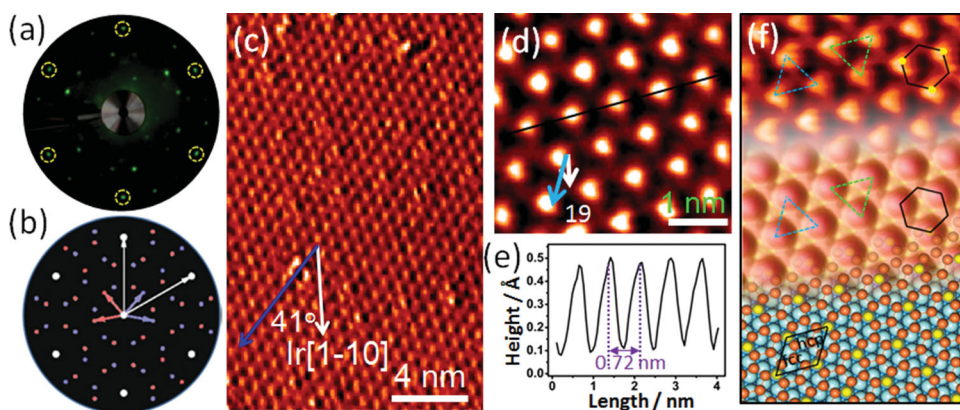
Figure 4. Silicene on Ir(111). (a) LEED patterns and (b) the corresponding schematic diagrams of the silicon superstructure formed on the Ir(111). (c) and (d) STM images showing two different ($\sqrt{7} \times \sqrt{7}$) superstructure domains of silicene on Ir(111). ($V_{bias} = -1.5$ V; $I = 0.25$ nA) (e) Line profile along the black line in (d), revealing the periodicity of the protrusions (0.72 nm) and a corrugation of around 0.4 Å for the silicene. (f) STM image (upper), simulated STM image (middle) and atomic model (lower) of buckled silicene on Ir(111). The rhombus indicates a unit cell. The triangles indicate the two different regions in a unit cell. The honeycomb feature is indicated by the black hexagon. Reproduced with permission.[61] (Copyright 2013, American Chemistry Society).

overlayer is about 0.6 Å, indicating that the silicene on Ir(111) is buckled.

In the high resolution STM image in Figure 4(f) upper part, the different regions of a unit cell are marked by upward and downward triangles. Three neighboring protrusions form a six-member ring, as is marked by the hexagon. Based on the STM results and DFT calculations, a model is proposed in Figure 4(f) lower part, in which the protruding silicon atoms are yellow and the other silicon atoms are orange. The unit cell of the $\sqrt{7} \times \sqrt{7}$ superstructure is indicated by the rhombus. There are six silicon atoms in one unit cell: one (yellow) sits on the top site; two sit at the hcp hollow and fcc hollow sites; the other three sit at the bridge sites. This model indicates that the silicon atoms are situated in different chemical environments with respect to the iridium surface, which is responsible for the overall geometric configuration of the buckled silicene on Ir(111). A simulated STM image is shown in Figure 4(f) middle part, which is nicely consistent with the experimental STM image.

Further electron localization function calculation implies that the interaction between silicon atoms is covalent bonding, while the interaction between silicon and iridium is mainly electrostatic. The above DFT calculation suggests that the interaction between silicene and Ir(111) is weaker than that between silicon atoms, therefore the intrinsic electronic structure of silicene is preserved. However, electronic structure of epitaxial silicene on Ir(111) needs to be further investigated experimentally, so as to find out whether the electronic dispersion resembling that of relativistic Dirac fermions at the K points of the Brillouin zone really exists or not.

3.2. Silicene on Ag(111)

The epitaxial silicene on Ag(111) is synthesized by directly depositing silicon onto Ag(111) surface while the substrate is maintained at around 250 °C.[59,62–64] The substrate temperature, deposition rate and silicon coverage are all important parameters for the formation of large scale defect-free silicene. If the temperature is outside a narrow range, the silicene either does not form at all or desorbs from the surface. The deposition rate plays an important role because it can affect the nucleation rate and growth rate of silicene. A recent DFT calculation by H. Shu et al. shows that on Ag(111) the silicene nucleation rate is very high compared to graphene nucleation on TM surfaces. The higher rate originates from the low diffusion barrier of Si atoms and the low nucleation barrier.[66] Therefore, higher deposition rates would lead to silicene samples that have smaller domains and more defects. In addition, the coverage of silicon is also important since an inappropriate value would lead to other silicon phases.

Although the silicene-Ag(111) system has been intensively studied in the past few years, many issues are still under debate. The synthesis of monolayer silicene was first reported by Lalmi et al. on the Ag(111) surface.[31] However, based on their experimental measurements, the reported lattice parameter of silicene was about 17% smaller than that of bulk silicon. Le Lay et al. later argued that such a small lattice is actually from clean Ag(111) (1×1) surface rather than silicene.[76] Vogt et al. claimed that they synthesized the monolayer silicene on Ag(111) for the first time, revealing a superstructure of (3×3) silicene on a (4×4) Ag(111) surface in STM images, as shown in **Figure 5**(a).[67] This result is supported by a number of following works.[71] Feng et al. also observed this phase, but they interpret it as a non-complete silicene stabilized by hydrogen with ordered holes (Figure 5(b)).[64] Instead, they propose the real monolayer silicene is in another phase with a honeycomb-like ($\sqrt{3} \times \sqrt{3}$) R30° superstructure, as shown in Figure 5(c). This structure was also reported by Resta et al. and other groups.[72–74] However, contrary to that by Feng et al., these works show that the ($\sqrt{3} \times \sqrt{3}$) R30° phase is always found on the thicker patch of the sample, indicating that it is actually multilayer silicene, as shown in Figure 5(d). Since the Si coverage and
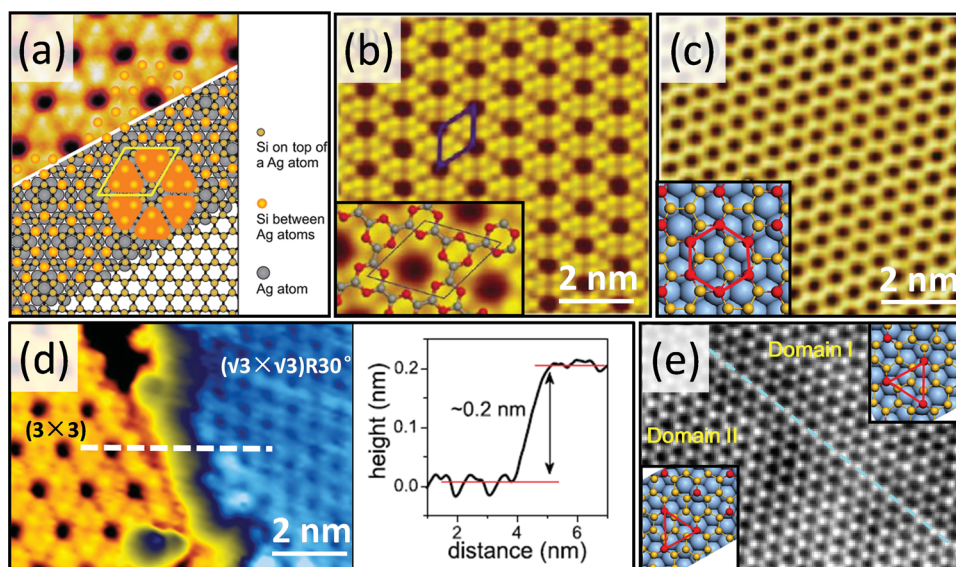
Figure 5. Silicene on Ag(111). (a)[67] (Copyright 2012, American Physics Society) (b)[64] (Copyright 2012, American Chemistry Society) STM images of the 3 × 3 superstructure of silicene on Ag(111) with two different structure models. (c) STM image and corresponding ball model of one monolayer silicene showing the ($\sqrt{3} \times \sqrt{3}$) R30° honeycomb superstructure. V_{bias} = 1.2 V, measurement temperature 77 K.[64] (Copyright 2012, American Chemistry Society) (d) STM image showing both the 3 × 3 and the ($\sqrt{3} \times \sqrt{3}$) R30° phases. The height profile along the white dashed line is shown on the right panal, indicating the ($\sqrt{3} \times \sqrt{3}$) R30° patch is higher than the 3 × 3 patch.[74] (Copyright 2013, American Institute of Physics) (e) STM image and corresponding ball models of the two energy-degenerated ($\sqrt{3} \times \sqrt{3}$) R30° rhombic superstructures domains of Silicene. V_{bias} = 0.1 V, measurement temperature 5 K.[65] (Copyright 2013, American Physics Society) All Reproduced with permission.

the Ag substrate temperature strongly affect the structure of the epitaxial silicene, various different structural phases have been identified by adjusting the growth conditions. Therefore, further detailed work on this system is needed in the future investigations.

Interestingly, Chen et al. found a phase transition of silicene on Ag(111).[65] At temperature above 40 K, silicene on Ag(111) is ($\sqrt{3} \times \sqrt{3}$) R30° honeycomb structure as we discussed before, however, below 40 K, it changes to two mirror-symmetric rhombic structures, which are boundary-separated but energy-degenerated, as shown in the STM images and the models in Figure 5(e). The energy barrier between these two mirror configurations were calculated not more than 38 meV, which enables the dynamic flip-flop motion that cannot be followed by STM at sample temperature higher than 40 K, resulting the ($\sqrt{3} \times \sqrt{3}$) R30° honeycomb structure in STM images. One must note that this interpretation is based on a monolayer silicene model. If the ($\sqrt{3} \times \sqrt{3}$) R30° phase appears on the multilayer silicene, as reported by Vogt et al.,[72,74] the dynamic flip-flop motion must originate from a weak inter-layer interaction, which requires further experimental investigation.

The graphene-like electronic structure of silicene on Ag(111), for example, linear electronic dispersion resembling that of relativistic Dirac fermions at the K points of the Brillouin zone, was reported by Vogt et al. based on angle-resolved photoemission spectroscopy measurements, and by Chen et al. based on STS measurements.[67,68] However, the exclusive assignment of the observed linear dispersion to silicene was questioned later because the influence of the Ag substrates was shown to be non-ignorable.[69] But the

linear dispersion should not be simply assigned to the Ag sp states either. Recently, it is demonstrated that this particular electronic structure actually arise due to the hybridization between silicene and Ag orbitals.[75] Very similar to the epitaxial graphene on TM, the epitaxial silicene also needs to be decoupled from the TM substrate for the future applications in electronic devices.

4. Hafnium Honeycomb Lattice on Ir(111)

Apart from the honeycomb lattice of graphene and silicene in which the atoms are bonded through the sp^2 hybridized *p* orbitals, the first pure metal epitaxial honeycomb lattice, of hafnium, was reported by L. Li et al. recently.[24] In this 2D lattice, which is supported on Ir(111) substrate, the atoms are connected mainly through d orbitals. The epitaxial hafnium honeycomb lattice is synthesized by depositing Hf on the clean Ir(111) surface at room temperature and post annealing at 300 °C.

The LEED pattern of the hafnium honeycomb lattice on Ir(111) sample shows a (2 × 2) superstructure with respect to the Ir(111) substrate [inset in **Figure 6**(a)]. The overview STM image in Figure 6(a) reveals a continuous 2D lattice of honeycomb structure. The orientation of the honeycomb lattice is parallel to the close-packed [1$\bar{1}$0] direction of the Ir(111) substrate. In the zoomed-in image in Figure 6(b), a perfect honeycomb structure is clearly resolved. The height profile curve in Figure 6(c) indicates a 5.40 Å periodicity of the honeycomb lattice, which is consistent with the (2 × 2) superstructure implied by the LEED pattern. Therefore, the
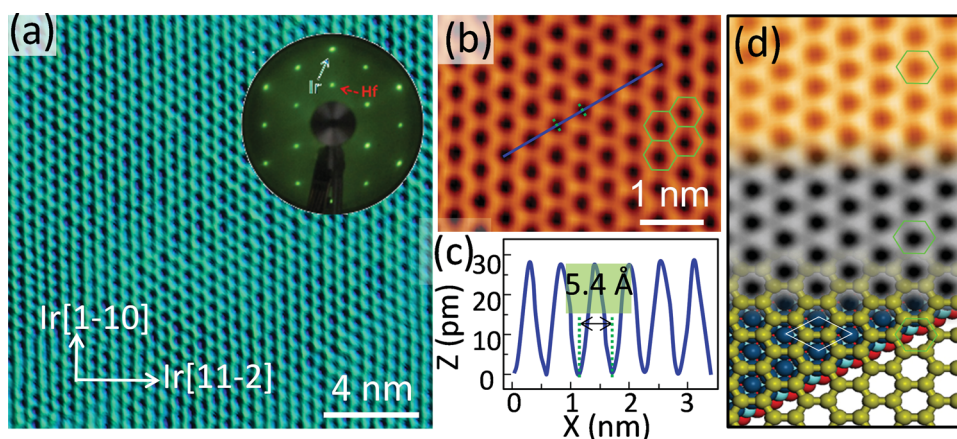
Figure 6. Honeycomb hafnium layer (hafnene) on Ir(111). (a) STM image, V_{bias} = −1.0 V; I = 0.8 nA. The inset LEED pattern reveals a 2 × 2 superstructure. (b) STM image shows the honeycomb lattice of Hf adlayer, V_{bias} = −0.7 V; I = 0.16 nA. (c) A height profile taken along the blue line in (b). The periodicity of the honeycomb lattice is 5.4 Å. (d) STM image (upper), simulated STM image (middle) and ball and stick model (lower) of Hf honeycomb lattice. The rhombus indicates a unit cell. The hexagons indicate the six member rings in the lattice. Reproduced with permission.[24] (Copyright 2013, American Chemistry Society).

Hf-Hf bond distance is determined to be 3.12 Å, which is very close to the Hf-Hf distance in the bulk. Such a close Hf-Hf distance in the honeycomb lattice indicates that the lattice is a compact graphene-like structure, instead of an ad-atom array on the substrate.

DFT calculation confirmed that the honeycomb lattice is a stable structure made of pure hafnium. The simulated STM image is consistent with the experimental one, as shown in Figure 6(d). On the other hand, a Hf-Ir alloy honeycomb lattice would produce an image which is completely different from the experimental one. Therefore, both experiment and theory suggest the existence of a continuous single-layer Hf film with honeycomb structure supported on the Ir(111) substrate, which may be called hafnene, as a special case of possible metalenes.[24]

Further calculations suggest that the Hf honeycomb lattice is metallic and strongly spin polarized (and hence ferromagnetic) with a magnetic moment of 1.46 μB per Hf atom. In addition, the calculation also suggests the presence of Dirac cones at the Fermi level near the K and K′ points of the Brillouin zone, which is very similar to the electronic structure of graphene.[5] It is estimated that the Fermi velocity of the cones is about 25% of that of graphene. The inclusion of the spin-orbit coupling, on the other hand, opens a gap at the Dirac point at the Fermi level by about 0.05 eV.

5. Conclusion and Outlook

Epitaxial growth is an effective method to synthesize a variety of 2D atomic crystals on TM substrates. The structure and quality of the 2D crystals can be influenced by many factors, including (1) the interaction of the crystal with its substrate, (2) the lattice mismatch, (3) the nucleation density in early stages of growth, (4) the source of the carbon atoms, (5) the growth rate, and so on. In the graphene-TM systems, the graphene-substrate interaction plays the major role. For example, the interaction is very strong for graphene

on Ru(0001), giving rise to nice single crystal graphene but highly coupled with the substrate. On the other hand, the interaction is weak for graphene on Pt(111), resulting in a rather less coupled graphene but with multiple domains. Therefore, a TM of intermediate interaction with graphene would be a better substrate, on which the crystalline and physical properties would both be preserved. Indeed, such a substrate is found in Ir(111), on which the graphene has large domains and a slightly rippled surface.

Ir(111) and Ag(111) are both good TM substrates for growing silicene. It seems silicene-Ag(111) is more complicated comparing with silicene-Ir(111), because multiple phases and small domains are formed. Particularly, a dynamic flip-flop motion is observed on the ($\sqrt{3} \times \sqrt{3}$)R30° phase of silicene on Ag(111) at room temperature, which can be attributed to a weak interaction of the top layer silicene with the substrate underneath. Since Ir(111) is a good substrate for both graphene and silicene due to its intermediate interaction with the supported overlayer, it is not surprising that a honeycomb structure of hafnium is also formed on such a substrate. We expect that on the TM substrates of intermediate interaction with the supported 2D crystals, more new 2D crystals could be found. So far, the research is mainly focus on the graphene-TM and silicene-TM systems. In future, other 2D crystal-TM systems should be explored. And, further work should be done on investigating the physical properties that are strongly desired for fundamental research and practical applications.

[1] K. S. Novoselov, D. Jiang, F. Schedin, T. J. Booth, V. V. Khotkevich, S. V. Morozov, A. K. Geim, *Proc. Natl. Acad. Sci. USA* **2005**, *102*, 10451.

[2] a) A. K. Geim, K. S. Novoselov, *Nat. Mater.* **2007**, *6*, 183; b) A. K. Geim, I. V. Grigorieva, *Nature* **2013**, *499*, 419.

[3] H. Shioyama, *J. Mater. Sci. Lett.* **2001**, *20*, 499.

[4] a) K. S. Novoselov, A. K. Geim, S. V. Morozov, D. Jiang, M. I. Katsnelson, I. V. Grigorieva, S. V. Dubonos, A. A. Firsov, *Nature* **2005**, *438*, 197; b) Y. B. Zhang, Y. W. Tan, H. L. Stormer, P. Kim, *Nature* **2005**, *438*, 201.

[5] A. H. C. Neto, F. Guinea, N. M. R. Peres, K. S. Novoselov, A. K. Geim, *Rev. Mod. Phys.* **2009**, *81*, 109.

[6] a) T. B. Martins, R. H. Miwa, A. J. R. da Silva, A. Fazzio, *Phys. Rev. Lett.* **2007**, *98*, 196803; b) Q. Yan, B. Huang, J. Yu, F. Zheng, J. Zang, J. Wu, B.-L. Gu, F. Liu, W. Duan, *Nano Lett.* **2007**, *7*, 1469; c) X. R. Wang, H. J. Dai, *Nat. Chem.* **2010**, *2*, 661.

[7] a) D. A. Abanin, L. S. Levitov, *Science* **2007**, *317*, 641; b) V. V. Cheianov, V. Fal'ko, B. L. Altshuler, *Science* **2007**, *315*, 1252.

[8] Y. B. Zhang, J. P. Small, W. V. Pontius, P. Kim, *Appl. Phys. Lett.* **2005**, *86*, 073104.

[9] a) F. Schedin, A. K. Geim, S. V. Morozov, E. W. Hill, P. Blake, M. I. Katsnelson, K. S. Novoselov, *Nat. Mater.* **2007**, *6*, 652; b) J. T. Robinson, F. K. Perkins, E. S. Snow, Z. Q. Wei, P. E. Sheehan, *Nano Lett.* **2008**, *8*, 3137; c) X. Wang, L. J. Zhi, K. Mullen, *Nano Lett.* **2008**, *8*, 323.

[10] K. S. Novoselov, A. K. Geim, S. V. Morozov, D. Jiang, Y. Zhang, S. V. Dubonos, I. V. Grigorieva, A. A. Firsov, *Science* **2004**, *306*, 666.

[11] M. Xu, T. Liang, M. Shi, H. Chen, *Chem. Rev.* **2013**, *113*, 3766.

[12] X. Zhang, Y. Xie, *Chem. Soc. Rev.* **2013**, *42*, 8187.

[13] S. Z. Butler, S. M. Hollen, L. Cao, Y. Cui, J. A. Gupta, H. R. Gutierrez, T. F. Heinz, S. S. Hong, J. Huang, A. F. Ismach, E. Johnston-Halperin, M. Kuno, V. V. Plashnitsa, R. D. Robinson, R. S. Ruoff, S. Salahuddin, J. Shan, L. Shi, M. G. Spencer, M. Terrones, W. Windl, J. E. Goldberger, *ACS Nano* **2013**, *7*, 2898.

[14] a) Y. Lin, J. W. Connell, *Nanoscale* **2012**, *4*, 6908; b) K. Raidongia, A. Nag, K. Hembram, U. V. Waghmare, R. Datta, C. N. R. Rao, *Chem. Eur. J.* **2010**, *16*, 149; c) D. C. Elias, R. R. Nair, T. M. G. Mohiuddin, S. V. Morozov, P. Blake, M. P. Halsall, A. C. Ferrari, D. W. Boukhvalov, M. I. Katsnelson, A. K. Geim, K. S. Novoselov, *Science* **2009**, *323*, 610.

[15] S. Stankovich, D. A. Dikin, G. H. B. Dommett, K. M. Kohlhaas, E. J. Zimney, E. A. Stach, R. D. Piner, S. T. Nguyen, R. S. Ruoff, *Nature* **2006**, *442*, 282.

[16] a) S. Stankovich, D. A. Dikin, R. D. Piner, K. A. Kohlhaas, A. Kleinhammes, Y. Jia, Y. Wu, S. T. Nguyen, R. S. Ruoff, *Carbon* **2007**, *45*, 1558; b) K. S. Kim, Y. Zhao, H. Jang, S. Y. Lee, J. M. Kim, J. H. Ahn, P. Kim, J. Y. Choi, B. H. Hong, *Nature* **2009**, *457*, 706.

[17] S. Bae, H. Kim, Y. Lee, X. F. Xu, J. S. Park, Y. Zheng, J. Balakrishnan, T. Lei, H. R. Kim, Y. I. Song, Y. J. Kim, K. S. Kim, B. Ozyilmaz, J. H. Ahn, B. H. Hong, S. Iijima, *Nat. Nanotechnol.* **2010**, *5*, 574.

[18] A. Kara, H. Enriquez, A. P. Seitsonen, L. Voon, S. Vizzini, B. Aufray, H. Oughaddou, *Surf. Sci. Rep.* **2012**, *67*, 1.

[19] a) M. D. Stoller, S. J. Park, Y. W. Zhu, J. H. An, R. S. Ruoff, *Nano Lett.* **2008**, *8*, 3498; b) A. M. Jones, H. Yu, N. J. Ghimire, S. Wu, G. Aivazian, J. S. Ross, B. Zhao, J. Yan, D. G. Mandrus, D. Xiao, W. Yao, X. Xu, *Nat. Nanotechnol.* **2013**, *8*, 634.

[20] a) A. Kumar, P. K. Ahluwalia, *Model. Simul. Mater. Sci.* **2013**, 21; b) D. Voiry, H. Yamaguchi, J. Li, R. Silva, D. C. B. Alves, T. Fujita, M. Chen, T. Asefa, V. B. Shenoy, G. Eda, M. Chhowalla, *Nat. Mater.* **2013**, *12*, 850.

[21] Y. Wang, C. Zhou, W. Wang, Y. Zhao, *Ind. Eng. Chem. Res.* **2013**, *52*, 4379.

[22] Q. H. Wang, K. Kalantar-Zadeh, A. Kis, J. N. Coleman, M. S. Strano, *Nat. Nanotechnol.* **2012**, *7*, 699.

[23] a) S. Lebegue, O. Eriksson, *Phys. Rev. B* **2009**, *79*, 115409; b) K. F. Mak, C. Lee, J. Hone, J. Shan, T. F. Heinz, *Phys. Rev. Lett.* **2010**, *105*, 136805; c) B. Radisavljevic, A. Radenovic, J. Brivio, V. Giacometti, A. Kis, *Nat. Nanotechnol.* **2011**, *6*, 147.

[24] L. Li, Y. Wang, S. Xie, X. B. Li, Y. Q. Wang, R. Wu, H. Sun, S. Zhang, H. J. Gao, *Nano lett.* **2013**, *13*, 4671.

[25] J. N. Coleman, M. Lotya, A. O'Neill, S. D. Bergin, P. J. King, U. Khan, K. Young, A. Gaucher, S. De, R. J. Smith, I. V. Shvets, S. K. Arora, G. Stanton, H. Y. Kim, K. Lee, G. T. Kim, G. S. Duesberg, T. Hallam, J. J. Boland, J. J. Wang, J. F. Donegan, J. C. Grunlan, G. Moriarty, A. Shmeliov, R. J. Nicholls, J. M. Perkins, E. M. Grieveson, K. Theuwissen, D. W. McComb, P. D. Nellist, V. Nicolosi, *Science* **2011**, *331*, 568.

[26] S. Park, R. S. Ruoff, *Nat. Nanotechnol.* **2009**, *4*, 217.

[27] J. Wintterlin, M. L. Bocquet, *Surf. Sci.* **2009**, *603*, 1841.

[28] J. M. Cai, P. Ruffieux, R. Jaafar, M. Bieri, T. Braun, S. Blankenburg, M. Muoth, A. P. Seitsonen, M. Saleh, X. L. Feng, K. Mullen, R. Fasel, *Nature* **2010**, *466*, 470.

[29] a) C. Berger, Z. M. Song, T. B. Li, X. B. Li, A. Y. Ogbazghi, R. Feng, Z. T. Dai, A. N. Marchenkov, E. H. Conrad, P. N. First, W. A. de Heer, *J. Phys. Chem. B* **2004**, *108*, 19912; b) G. M. Rutter, J. N. Crain, N. P. Guisinger, T. Li, P. N. First, J. A. Stroscio, *Science* **2007**, *317*, 219; c) A. Fleurence, R. Friedlein, T. Ozaki, H. Kawai, Y. Wang, Y. Yamada-Takamura, *Phys. Rev. Lett.* **2012**, *108*, 245501; d) A. Grueneis, K. Kummer, D. V. Vyalikh, *New J. Phys.* **2009**, *11*, 073050; e) J. Coraux, T. N. Plasa, C. Busse, T. Michely, *New J. Phys.* **2008**, *10*, 043033; f) A. Varykhalov, O. Rader, *Phys. Rev. B* **2009**, *80*, 035437; g) C. Klink, I. Stensgaard, F. Besenbacher, E. Lægsgaard, *Surf. Sci.* **1995**, *342*, 250; h) J. -H. Gao, N. Ishida, I. Scott, D. Fujit, *Carbon* **2012**, *50*, 1674.

[30] A. Kara, C. Leandri, M. E. Davila, P. D. Padova, B. Ealet, H. Oughaddou, B. Aufray, G. L. Lay, *J Supercond. Nov. Magn.* **2009**, *22*, 259.

[31] B. Lalmi, H. Oughaddou, H. Enriquez, A. Kara, S. Vizzini, B. Ealet, B. Aufray, *Appl. Phys. Lett.* **2010**, *97*, 223109.

[32] S. Marchini, S. Guenther, J. Wintterlin, *Phys. Rev. B* **2007**, *76*, 075429.

[33] E. Loginova, N. C. Bartelt, P. J. Feibelman, K. F. McCarty, *New J. Phys.* **2009**, *11*, 063046.

[34] A. Reina, X. T. Jia, J. Ho, D. Nezich, H. B. Son, V. Bulovic, M. S. Dresselhaus, J. Kong, *Nano lett.* **2009**, *9*, 30.

[35] L. B. Gao, W. C. Ren, H. L. Xu, L. Jin, Z. X. Wang, T. Ma, L. P. Ma, Z. Y. Zhang, Q. Fu, L. M. Peng, X. H. Bao, H. M. Cheng, *Nat. Commun.* **2012**, *3*, 699.

[36] X. S. Li, W. W. Cai, J. H. An, S. Kim, J. Nah, D. X. Yang, R. Piner, A. Velamakanni, I. Jung, E. Tutuc, S. K. Banerjee, L. Colombo, R. S. Ruoff, *Science* **2009**, *324*, 1312.

[37] X. S. Li, Y. W. Zhu, W. W. Cai, M. Borysiak, B. Y. Han, D. Chen, R. D. Piner, L. Colombo, R. S. Ruoff, *Nano lett.* **2009**, *9*, 4359.

[38] a) H. J. Gao, L. Gao, *Prog. Surf. Sci.* **2010**, *85*, 28; b) H.-J. Gao, K. Sohlberg, Z. Q. Xue, H. Y. Chen, S. M. Hou, L. P. Ma, X. W , Fang, S. J. Pang, S. J. Pennycook, *Phys. Rev. Lett.* **2000**, *84*, 1780.

[39] a) S. Hagstrom, H. B. Lyon, G. A. Somorjai, *Phys. Rev. Lett.* **1965**, *15*, 491; b) S. D. Robertson, *Carbon* **1970**, *8*, 365; c) S. D. Robertson, *Carbon* **1972**, *10*, 221.

[40] a) Y. Pan, D.-X. Shi, H.-J. Gao, *Chin. Phys.* **2007**, *16*, 3151; b) T. W. Ebbesen, H. Hiura, *Adv. Mater.* **1995**, *7*, 582.

[41] Y. Pan, H. Zhang, D. Shi, J. Sun, S. Du, F. Liu, H. Gao, *Adv. Mater.* **2009**, *21*, 2777.

[42] E. N. Voloshina, Y. S. Dedkov, S. Torbruegge, A. Thissen, M. Fonin, *Appl. Phys. Lett.* **2012**, *100*, 241606.

[43] M. Gao, Y. Pan, L. Huang, H. Hu, L. Zhang, H. Guo, S. Du, H. Gao, *Appl. Phys. Lett.* **2011**, *98*, 033101.

[44] A. T. N'Diaye, S. Bleikamp, P. J. Feibelman, T. Michely, *Phys. Rev. Lett.* **2006**, *97*, 215501.

[45] J. Cho, L. Gao, J. F. Tian, H. L. Cao, W. Wu, Q. K. Yu, E. N. Yitamben, B. Fisher, J. R. Guest, Y. P. Chen, N. P. Guisinger, *ACS Nano* **2011**, *5*, 3607.

[46] a) L. Huang, Y. Pan, L. Pan, M. Gao, W. Xu, Y. Que, H. Zhou, Y. Wang, S. Du, H.-J. Gao, *Appl. Phys. Lett.* **2011**, *99*, 163107; b) J. H. Mao, L. Huang, Y. Pan, M. Gao, J. F. He, H. T. Zhou, H. M. Guo, Y. Tian, Q. Zou, L. Z. Zhang, H. G. Zhang, Y. L. Wang, S. X. Du, X. J. Zhou, A. H. C. Neto, H. J. Gao, *Appl. Phys. Lett.* **2012**, *100*, 093101; c) L. Huang, W. Y. Xu, Y. D. Que, J. H. Mao, L. Meng, L. D. Pan, G. Li, Y. L. Wang, S. X. Du, Y. Q. Liu, H. J. Gao, *Chin. Phys. B* **2013**, *22*, 096803; d) L. F. Li, Y. L. Wang, L. Meng, R. T. Wu, H. J. Gao, *Appl. Phys. Lett.* **2013**, *102*, 093106; e) G. Li et al., unpublished results.

[47] L. Meng, R. Wu, H. Zhou, G. Li, Y. Zhang, L. Li, Y. Wang, H. J. Gao, *Appl. Phys. Lett.* **2012**, *100*, 083101.

[48] A. B. Preobrajenski, M. L. Ng, A. S. Vinogradov, N. Martensson, *Phys. Rev. B* **2008**, *78*, 073401.

[49] T. A. Land, T. Michely, R. J. Behm, J. C. Hemminger, G. Comsa, *Surf. Sci.* **1992**, *264*, 261.

[50] P. Sutter, J. T. Sadowski, E. Sutter, *Phys. Rev. B* **2009**, *80*, 245411.

[51] R. Rosei, S. Modesti, F. Sette, *Phys. Rev. B* **1984**, *29*, 3416.

[52] P. W. Sutter, J. I. Flege, E. A. Sutter, *Nat. Mater.* **2008**, *7*, 406.

[53] N. C. Bartelt, K. F. McCarty, *MRS Bull.* **2012**, *37*, 1158.

[54] B. Wang, M. L. Bocquet, S. Marchini, S. Gunther, J. Wintterlin, *Phys. Chem. Chem. Phys.* **2008**, *10*, 3530.

[55] a) H. G. Zhang, J. T. Sun, T. Low, L. Z. Zhang, Y. Pan, Q. Liu, J. H. Mao, H. T. Zhou, H. M. Guo, S. X. Du, F. Guinea, H.-J. Gao, *Phys. Rev. B* **2011**, *84*, 245436; b) Y. Pan, M. Gao, L. Huang, F. Liu, H. Gao, *Appl. Phys. Lett.* **2009**, *95*, 093106; c) G. Li, H. T. Zhou, L. D. Pan, Y. Zhang, J. H. Mao, Q. Zou, H. M. Guo, Y. L. Wang, S. X. Du, H. J. Gao, *Appl. Phys. Lett.* **2012**, *100*, 013304; d) H. T. Zhou, J. H. Mao, G. Li, Y. L. Wang, X. L. Feng, S. X. Du, K. Mullen, H. J. Gao, *Appl. Phys. Lett.* **2011**, *99*, 153101.

[56] C.-C. Liu, W. Feng, Y. Yao, *Phys. Rev. Lett.* **2011**, *107*, 076802.

[57] G. G. Guzman-Verri, L. C. L. Y. Voon, *Phys. Rev. B* **2007**, *76*, 075131.

[58] a) G. Le Lay, B. Aufray, C. Leandri, H. Oughaddou, J. P. Biberian, P. De Padova, M. E. Davila, B. Ealet, A. Kara, *Appl. Surf. Sci.* **2009**, *256*, 524; b) P. De Padova, O. Kubo, B. Oivieri, C. Quaresima, T. Nakayama, M. Aono, G. Le Lay, *Nano lett.* **2012**, *12*, 5500.

[59] a) B. Aufray, A. Kara, S. Vizzini, H. Oughaddou, C. Leandri, B. Ealet, G. Le Lay, *Appl. Phys. Lett.* **2010**, *96*, 056804; b) P. De Padova, C. Quaresima, C. Ottaviani, P. M. Sheverdyaeva, P. Moras, C. Carbone, D. Topwal, B. Olivieri, A. Kara, H. Oughaddou, B. Aufray, G. Le Lay, *Appl. Phys. Lett.* **2010**, *96*, 261905.

[60] S. Cahangirov, M. Topsakal, E. Akturk, H. Sahin, S. Ciraci, *Phys. Rev. Lett.* **2009**, *102*, 236804.

[61] L. Meng, Y. L. Wang, L. Z. Zhang, S. X. Du, R. T. Wu, L. F. Li, Y. Zhang, G. Li, H. T. Zhou, W. A. Hofer, H. J. Gao, *Nano lett.* **2013**, *13*, 685.

[62] a) L. Chen, C.-C. Liu, B. Feng, X. He, P. Cheng, Z. Ding, S. Meng, Y. Yao, K. Wu, *Phys. Rev. Lett.* **2012**, *109*, 056804; b) H. Jamgotchian, Y. Colignon, N. Hamzaoui, B. Ealet, J. Y. Hoarau, B. Aufray, J. P. Biberian, *J. Phys.: Condens. Matter* **2012**, *24*, 172001; c) C.-L. Lin, R. Arafune, K. Kawahara, N. Tsukahara, E. Minamitani, Y. Kim, N. Takagi, M. Kawai, *Appl. Phys. Express*

2012, *5*, 045802; d) R. Arafune, C.-L. Lin, K. Kawahara, N. Tsukahara, E. Minamitani, Y. Kim, N. Takagi, M. Kawai, *Surf. Sci.* **2013**, *608*, 297; e) Z. Majzik, M. R. Tchalala, M. Svec, P. Hapala, H. Enriquez, A. Kara, A. J. Mayne, G. Dujardin, P. Jelinek, H. Oughaddou, *J. Phys.: Condens. Matter* **2013**, *25*, 225301; f) A. Resta, T. Leoni, C. Barth, A. Ranguis, C. Becker, T. Bruhn, P. Vogt, G. Le Lay, *Sci. Rep.* **2013**, *3*, 2399.

[63] H. Enriquez, S. Vizzini, A. Kara, B. Lalmi, H. Oughaddou, *J. Phys.: Condens. Matter* **2012**, *24*, 314211.

[64] B. Feng, Z. Ding, S. Meng, Y. Yao, X. He, P. Cheng, L. Chen, K. Wu, *Nano lett.* **2012**, *12*, 3507.

[65] L. Chen, H. Li, B. J. Feng, Z. J. Ding, J. L. Qiu, P. Cheng, K. H. Wu, S. Meng, *Phys. Rev. Lett.* **2013**, *110*, 085504.

[66] H. Shu, D. Cao, P. Liang, X. Wang, X. Chen, W. Lu, *Phys. Chem. Chem. Phys.* **2014**, *16*, 304. DOI: 10.1039/C3CP53933D.

[67] P. Vogt, P. De Padova, C. Quaresima, J. Avila, E. Frantzeskakis, M. C. Asensio, A. Resta, B. Ealet, G. Le Lay, *Phys. Rev. Lett.* **2012**, *108*, 155501.

[68] L. Chen, C.-C. Liu, B. Feng, X. He, P. Cheng, Z. Ding, S. Meng, Y. Yao, K. Wu, *Phys. Rev. Lett.* **2012**, *109*, 056804

[69] a) Z. X. Guo, S. Furuya, J. I. Iwata, A. Oshiyama, *J. Phys. Soc. Jpn.* **2013**, *82*, 063714; b) R. Arafune, C. L Lin, R. Nagao, M. Kawai, N. Takagi, *Phys. Rev. Lett.* **2013**, *110*, 229701; c) C. L. Lin, R. Arafune, K. Kawahara, M. Kanno, N. Tsukahara, E. Minamitani, Y. Kim, M. Kawai, N. Takagi, *Phys. Rev. Lett.* **2013**, *110*, 076801; d) P. Gori, O. Pulci, F. Ronci, S. Colonna, F. Bechstedt, *J Appl. Phys.* **2013**, *114*, 113710.

[70] Y. Hao, M. S. Bharathi, L. Wang, Y. Liu, H. Chen, S. Nie, X. Wang, H. Chou, C. Tan, B. Fallahazad, H. Ramanarayan, C. W. Magnuson, E. Tutuc, B. I. Yakobson, K. F. McCarty, Y.-W. Zhang, P. Kim, J. Hone, L. Colombo, R. S. Ruoff, *Science* **2013**, *342*, 720.

[71] a) S. Cahangirov, M. Audiffred, P. Tang, A. Iacomino, W. Duan, G. Merino, A. Rubio, *Phys. Rev. B* **2013**, *88*, 035432; b) D. Kaltsas, L. Tsetseris, A. Dimoulas, *J. Phys.: Condens. Matter* **2012**, *24*, 442001; c) Y. Fukaya, I. Mochizuki, M. Maekawa, K. Wada, T. Hyodo, I. Matsuda, A. Kawasuso, *Phys. Rev. B* **2013**, *88*, 205413; d) D. Chiappe, C. Grazianetti, G. Tallarida, M. Fanciulli, A. Molle, *Adv. Mater.* **2012**, *24*, 5088; e) J. Gao, J. Zhao, *Sci. Rep.* **2012**, *2*, 1.

[72] A. Resta, T. Leoni, C. Barth, A. Ranguis, C. Becker, T. Bruhn, P. Vogt, G. Le Lay, *Sci. Rep.* **2013**, *3*, 2399

[73] P. De Padova, P. Vogt, A. Resta, J. Avila, I. Razado-Colambo, C. Quaresima, C. Ottaviano, B. Olivieri, T. Bruhn, T. Hirahara, T. Shirai, S. Hasegawa, M. C. Asensio, G. Le Lay, *Appl. Phys. Lett.* **2013**, *102*, 163106.

[74] P. Vogt, P. Capiod, M. Berthe, A. Resta, P. De Padova, T. Bruhn, G. Le Lay, B. Grandidier, *Appl. Phys. Lett.* **2014**, *104*, 021602.

[75] a) S. Cahangirov, M. Audiffred, P. Tang, A. Iacomino, W. Duan, G. Merino, A. Rubio, *Phys. Rev. B* **2013**, *88*, 035432; b) D. Tsoutsou, E. Xenogiannopoulou, E. Golias, P. Tsipas, A. Dimoulas, *Appl. Phys. Lett.* **2013**, *103*, 231604.

[76] G. Le Lay, P. De Padova, A. Resta, T. Bruhn, P. Vogt, *J. Phys. D: Appl. Phys.* **2012**, *45*, 392001.